

9111010111116

roughness and soil moisture (Liu et al., 2010). For example, the Weather Research and Forecasting model coupled with Chemistry (WRF-Chem) (Grell et al., 2005) and with the GOCART aerosol scheme (Ginoux et al., 2001) has been applied to simulate dust emission over central East Asia (Kumar et al., 2014), the United States (Zhao et al., 2010), and East Asia (Chen et al., 2013). The Barcelona Supercomputing Centre (BSC) BSC-DREAM8b regional model has been previously applied over North Africa and South Europe to assess the contribution of desert dust to particulate matter levels over Portugal (Monteiro et al., 2015). Another example is the NMMB/BSC-Dust model (Pérez et al., 2011; Haustein et al., 2012), an online multiscale atmospheric model designed and developed at the BSC in collaboration with NOAA/NCEP, NASA Goddard Institute for Space Studies and the International Research Institute for Climate and Society (IRI), which is intended to provide short to medium-range dust forecasts for both regional and global domains. These three models (BSC-DREAM8b, WRF-Chem and NMMB/BSC-Dust) are included in the Sand and Dust Storm Warning, Advisory and Assessment System established by the World Meteorological Organisation (WMO), which provides operational forecasts of mineral dust dispersion over North Africa, Middle East, and Europe.

The CHIMERE (Menut et al., 2013) model and the EURAD-IM (EURopean Air pollution Dispersion - Inverse Model, Elbern et al., 2007) models are mesoscale Eulerian models that compute transport, chemical reactions and deposition of gas-phase and aerosol species in a non-hydrostatic configuration. Both models are being used, since more than 10 years, for air quality operational purposes in Portugal (CHI-MERE) and Germany (EURAD-IM) and both models have a dust module encoded which needs proper evaluation to support the daily dust prediction. Additionally, they are state-of-the art chemical transport models (CTM) being part of the Copernicus Atmosphere Monitoring Service, providing daily air quality forecast over Europe and reanalysis. The development of the CHIMERE dust module started in 2005 (Vautard et al., 2005) with continuous updates and reformulations since then (Mailler et al., 2017; Menut et al., 2007). The last developments comprehended the extension of the dust production module to any domain over the globe; the addition of a MODIS erodibility database for arid areas, and also the inclusion of Kok's production model (Kok et al., 2014). As EURAD-IM is mainly used for scientific research purposes, it is in constant development by the team of the Rhenish Institute for Environmental Research at the University of Cologne (Elbern et al., 2010; Elbern and Strunk, 2006; Schroedter-Homscheidt et al., 2010). The mineral dust emission module included in EURAD-IM is based on Nickovic et al. (2001). It estimates the mineral dust emissions driven by the meteorological and surface information. Recently, this module was updated in order to calculate mineral dust concentrations in two particle size modes (diameter, d): the coarse mode $(d \ge 1 \, \mu m)$ and the accumulation mode $(0.1 \le d < 1 \, \mu m)$ (Friese et al.,

The objective of this study is to evaluate and test the capability of the dust modules encoded in both CTM to reproduce dust transport and their impacts on PM10 and aerosol optical properties. This paper focuses on one strong dust episode reaching the Iberian Peninsula, occurring on 19–23 February 2016. The results of the model simulations are evaluated with measured PM10 concentrations from the Portuguese air quality monitoring network, AOD from Aerosol Robotic Network (AERONET) sun/sky radiometer measurements, and Dust Red-Green-Blue (RGB) composites, which are based on satellite observations.

The EURAD-IM system comprehends the Modal Aerosol Dynamics model for Europe (MADE, Ackermann et al., 1998) that describes the physical and chemical processes of particle species in the troposphere (off-line mode). The aerosol particle size distribution is modelled using the modal concept: fine particles are treated by two interacting subdistributions, and the third mode is formed by coarse particles (logwith distributions diameters $d_{Aitken} = 0.01 \, \mu m$ $d_{accumulation} = 0.07\,\mu m, \text{ and } d_{coarse} = 1.0\,\mu m$ and standard deviations σ_{Aitken} = 1.7, $\sigma_{Accumulation}$ = 2.0, and σ_{coarse} = 2.2). The Aitken mode represents secondary aerosols from fresh particles by nucleation, while the accumulation mode includes aged particles as well as directly emitted species, which are also represented in the coarse mode. The latter includes sea salt, wind-blown dust and particles from different anthropogenic emission sources. Mineral dust concentrations are calculated in the coarse and accumulation modes.

Within EURAD-IM, the simulation of mineral dust emissions follows the methodology developed by Nickovic et al. (2001), which is applied to grid cells with a desert surface fraction from the United States Geological Survey (USGS) database, greater or equals than 0.1% (desert/no-desert mask). The dust emissions are calculated from the turbulence flux of mineral dust that depends on the stability of the nearsurface atmosphere and the soil conditions. The frictional wind velocity is taken by the dust module to define the stability of the near-surface atmosphere. The soil condition is determined by the contribution of Cosby soil types (sand, silt large, silt small and clay) for each ZOBLER texture classes (coarse, medium, fine, coarse-medium, coarse-fine, medium-fine and coarse-medium-fine), as well as by soil moisture content and the type of vegetation cover. The meteorological and hydrological conditions simulated by the WRF model are used to calculate the effective rates of the injected dust concentration and sinks, controlled by dry and wet deposition, as well as the horizontal and vertical advection (Tegen and Fung, 1994; Nickovic et al., 2001).

2.2. The CHIMERE dust module

The aerosol module of CHIMERE model was implemented in 2004 (Bessagnet et al., 2004) with further improvements concerning the dust natural emissions and re-suspension over Europe (Vautard et al., 2005; Hodzic et al., 2006; Bessagnet et al., 2008). The calculation of the mineral dust emissions requires several surface and soil databases. Since the 2016a version, these databases are global, which allows for the calculation of mineral dust emissions in every location on the globe. Like EURAD-IM, CHIMERE operates in off-line mode as well.

In CHIMERE, a desert mask is used, specifying what surface is potentially erodible. This mask corresponds to the areas classified as scrublands or barren soil in the USGS land use dataset. The mineral dust flux calculation is performed for potentially erodible areas and it includes parameterisations taking into account wind speed, precipitation and soil characteristics. The mineral dust flux can be calculated according to schemes of Marticorena and Bergametti (1995), Alfaro and Gomes (2001), or Kok et al. (2014). In this work, the optimized version of the Alfaro and Gomes (2001) scheme is used. It computes sand-blasting fluxes based on the partitioning of the kinetic energy of individual saltating aggregates and the cohesion energy of populations of dust particles. This dust production model assumes that dust emitted by sandblasting is characterized by three modes (log-normal distributions with diameters $d_1 = 1.5 \,\mu\text{m}$, $d_2 = 6.7 \,\mu\text{m}$, and $d_3 = 14.2 \,\mu\text{m}$ and

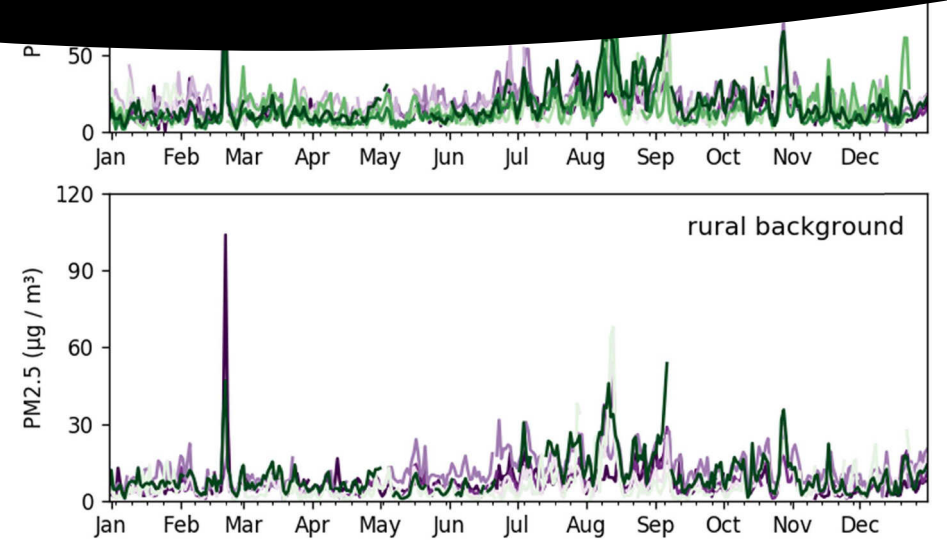


Fig. 1. Daily PM10 and PM2.5 concentrations observed at rural background monitoring stations from the Portuguese monitoring network, during 2016.

standard deviations $\sigma_1 = 1.7$, $\sigma_2 = 1.6$, and $\sigma_3 = 1.5$), whose emitted proportion depends on the wind friction velocity. As soil aggregate size or wind speed increases, kinetic energy becomes able to release first particles of the coarsest mode that are associated with the lowest cohesion energy, then particles from the intermediate population, and finally the finest particles.

3. Modelling a dust episode

In this section the selection of a specific dust episode is presented and justified, together with the modelling setups used for the simulations.

3.1. The selected dust episode

In late February 2016, a strong mineral dust episode occurred, affecting roughly all background air quality monitoring stations in mainland Portugal. This episode was due to a vast plume of sand and dust blown northward from the Sahara Desert (Cazorla et al., 2017). Fig. 1 shows the time series of daily PM10 and PM2.5 concentrations observed at rural background monitoring stations in Portugal during the year 2016. Remarkably high PM10 and PM2.5 concentrations of up to $175\,\mu g\,m^{-3}$ and $105\,\mu g\,m^{-3}$, respectively, were measured on 22–23 February. Although the event was extreme in terms of PM concentrations, it just lasted for about 2 day at each monitoring station.

In general, large-scale transport from the Sahara to the Iberian Peninsula requires a meridional deflection of the large-scale atmospheric flow. There are various case studies and long-term investigations about typical transport pathways of Saharan dust (e.g. Escudero et al., 2005; Meloni et al., 2008; Israelevich et al., 2012; Salvador et al., 2014) indicating that it is a variety of synoptic patterns which lead to dust episodes in Europe. Following these studies, the dominant meteorological conditions required for dust episodes to appear over Europe are either a ridge over north/north-eastern Africa, a trough over the western coast of North-Africa/Portugal, or a combination of both.

The meteorological situation during the chosen Saharan dust episode is dominated by a low-pressure system located at the north-

western coast of Africa, which led to the typical transport pathway that characterizes Saharan dust episodes over the Iberian Peninsula (Escudero et al., 2005; Cazorla et al., 2017). Since the beginning of the process on 19 February, this cut-off low was stationary with its centre being located above the coast of Morocco.

Fig. 2 shows the synoptic situation on 21 February 2016, 00 UTC as forecasted by the WRF model. The presence of the cut-off low induces a strong meridional transport of air from Algeria straight towards eastern

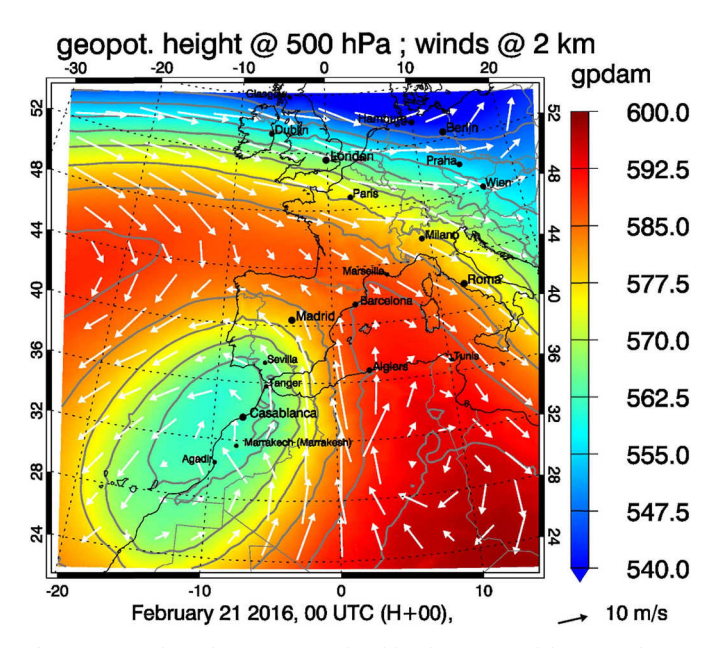


Fig. 2. Meteorological situation simulated by the WRF model on 21 February 2016, 00UTC. Shown is the geopotential height in 500 hPa (color coded) and horizontal winds on a sigma-level referring to 2 km above sea level (white arrows). The length of each wind vector is proportional to the horizontal wind speed (scale at bottom right). (For interpretation of the references to colour in this figure legend, the reader is referred to the Web version of this article.)

ornes (strength) which is

Land surface	Noah Land Surface Model			
Planetary boundary layer (PBL)	MYNN Level 2.5 PBL			
Cumulus	Grell-Freitas (GF) scheme			
	EURAD-IM	CHIMERE		
Clouds	Roselle and Binkowski (1999) R2.6			
Dry deposition	Zhang et al. (2003) scheme	Zhang et al. (2001)		
Advection	Bott (1989) algorithm	The 2nd order Van Leer scheme (Van Leer, 1979)		
Aerosol dynamics	MADE including Analytical Predictor for Condensation (APC) and High Dimensional Model Representation (HDMR) (Nieradzik, 2005)			

parts of the Iberian Peninsula. Here, forecasted wind speeds in typical dust transport altitudes of about 2 km altitude reached up to 25 m/s. Furthermore, the closed cyclonic flow around the cut-off leads to mainly westward transport from Spain towards Portugal. During the second half of this day, the cut-off low starts to move north-westerly. Its centre is located above the Iberian Peninsula on 22 February leading to weak winds in this area. Finally, the cut-off reconnects to the general westward-moving circulation on 23 February and vanishes slowly.

3.2. Modelling setup

To compare the performance of both CTMs with their individual mineral dust modules, both, CHIMERE and EURAD-IM modelling systems simulate the selected episode (21-25 February 2016) using six days of spin-up (starting on 15 February) and utilizing the same meteorological conditions provided by the WRF simulations (Table 1). Here, boundary and initial conditions from ECMWF re-analysis at 0.225° horizontal resolution are used. The common simulation domain covers the source areas in the Sahara Desert and the dust affected area (South-West and Central Europe) with an extension of 3753 km in W-E and N-S directions. Fig. 3 displays the selected domain, whose grid has a horizontal resolution of $27 \times 27 \, \text{km}^2$ and is vertically defined by 23 sigma layers distributed up to 100 hPa for WRF and EURAD-IM, and by 24 sigma layers to 200 hPa in case of CHIMERE. In addition to the mineral dust emissions computed by both CTMs, the simulations include anthropogenic emission data from TNO inventory (Kuenen et al., 2014).

Table 1 summarizes the main differences of the CTMs regarding the physical schemes, which are responsible for the dust transport. It is expected that even the models are using different advection schemes, the individual simulated transport patterns of each model behave similar, as the advection is controlled by the same meteorological driver.

4. Results and discussion

Both modelling results (EURAD-IM and CHIMERE outputs) are firstly compared in terms of the emission source region and emission strength. The horizontal transport is evaluated qualitatively comparing the models' dust dispersion in terms of AOD fields with SEVIRI (Spinning Enhanced Visible and Infrared Imager) RGB product images. The results are then analysed taking into account in-situ observations, such as PM10 and PM2.5 surface concentrations at specific locations in Portugal, as well as remote-sensing AOD observations from AERONET.

duction (see section 2). While the dust source regions within EURAD-IM are concentrated in northern Algeria with strongest emissions on the Moroccan-Algerian border, and few emissions also in south-east Algeria, CHIMERE considers dust sources in numerous regional patches distributed all over Algeria and neighbouring countries. CHIMERE accounts most emissions within the area of the Grand Erg Occidental.

The discrepancy between the emissions of both CTMs is due to the different dust production models employed by each model: Nickovic et al. (2001) in the case of EURAD-IM and Alfaro and Gomes (2001) in CHIMERE. According to EURAD-IM, dust is mainly emitted by loam soils, while CHIMERE predicts more emissions from sandy soils. In fact, silty soils are, in EURAD-IM, more vulnerable for uplift (γ [%]) than sandy soils (γ _{sand} = 12%; γ _{silt} = 100%). The comparison of the soil types of Fig. 3 and the source regions of Fig. 4 therefore illustrates the strong correlation between soil properties and mineral dust emissions.

4.2. Spatial analysis

To characterize and evaluate the spatial extension and evolution of the desert dust outbreak, SEVIRI's false colour Dust-RGB product is used. The RGB composite is based on infrared channel data, which is borne by the geostationary MSG (Meteosat Second Generation) satellite. Among other objectives SEVIRI was designed by EUMETSAT (European Organisation for the Exploitation of Meteorological Satellites) to monitor the evolution of dust storms during both, day and night. The Dust-RGB makes use of the brightness temperature differences between the channels that are close to IR windows of $8.7\,\mu m$, $10.8\,\mu m$, and $12.0\,\mu m$ (Lensky and Rosenfeld, 2008). The resulting product depicts dust in magenta and purple colours over land, depending on daytime or nighttime conditions, respectively. A dusty atmosphere can also be tracked over water by magenta colouring. Cold, thick, high-level clouds have red-brown tones and thin cirrus clouds appear very dark, nearly black.

The evolution of the dust outbreak from 20 to 22 February 2016 is illustrated in Fig. 5. Here, a sequence of the false colour Dust-RGB images is shown in comparison with the AOD at 550 nm wavelength simulated by both models (Fig. 5). The general mineral dust transport from the source regions towards the Iberian Peninsula behaves very similar, examining both the RGB satellite data and the EURAD-IM and CHIMERE model results.

On 20 February at 16 UTC, a dust hotspot is highlighted in the Moroccan-Algerian border along the Atlas Mountains. According to Cazorla et al. (2017), no significant visibility reduction was reported in the north-facing slope areas of the Tell Atlas and in the Rif Mountains at the coast of Algeria and Morocco. This indicates that dust was lifted into higher atmospheric levels before passing over the northern slope of the Atlas Mountains and the North African coast.

During the 21 February, the dust layer starts to enter Spain passing over Malaga. During the afternoon, the dust cloud continues to drift northbound, while also spreading westerly and therefore affecting Portugal. On the 22 February, at 00 UTC, the dust cloud is located mainly in Spain and Portugal, while the dust uptake into the atmosphere in North Africa vanishes. Later, transported dust dissipates north and westwards.

The comparison of modelled optical depths with Dust-RGB maps shows a good qualitative performance of both models simulating this event. However, CHIMERE estimates a more durable and wide spread plume of dust over Iberian Peninsula, which is not visible in the RGB

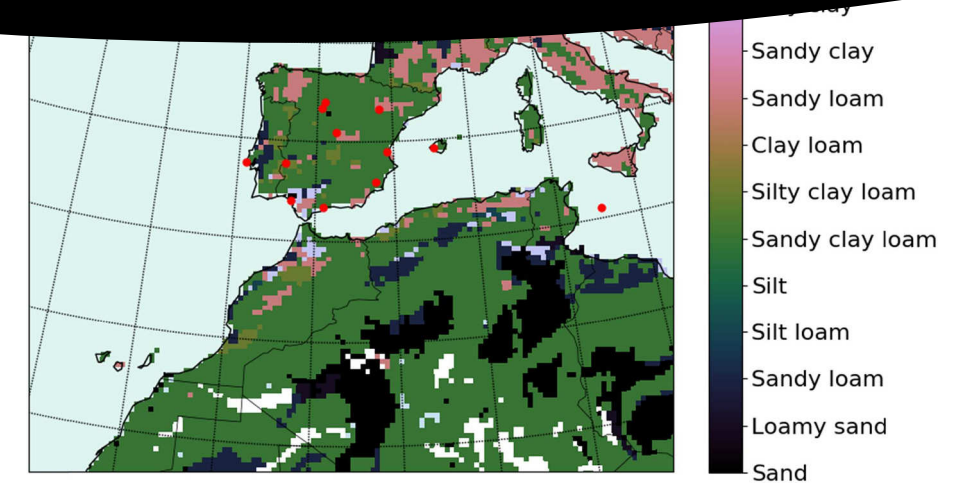


Fig. 3. Simulation domain ($27 \text{ km} \times 27 \text{ km}$, horizontal resolution), soil types and the location of the AERONET stations (red dots). (For interpretation of the references to colour in this figure legend, the reader is referred to the Web version of this article.)

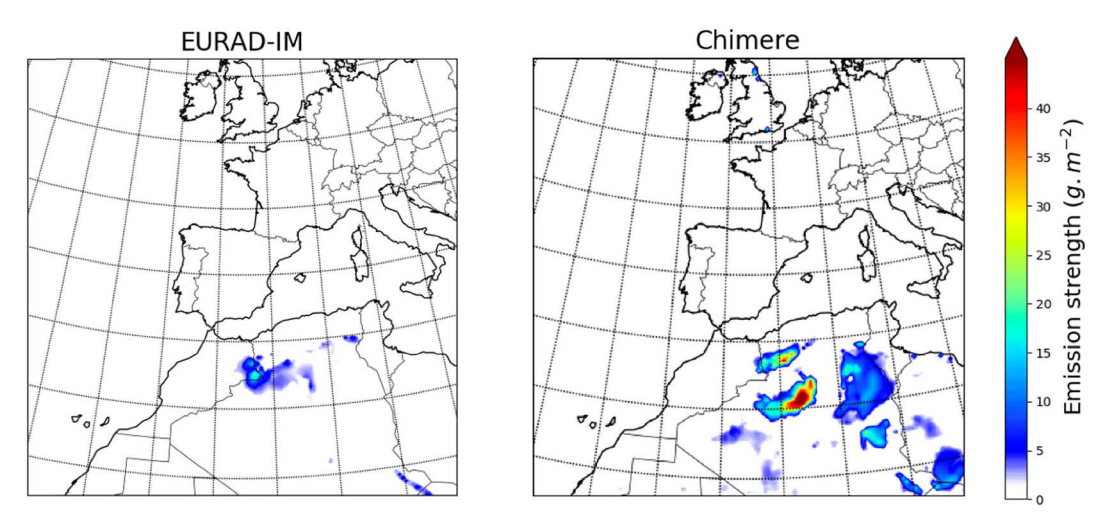


Fig. 4. Dust emissions computed by EURAD-IM and CHIMERE models, integrated over time (from 20 to 25 February 2016).

product nor in the EURAD-IM modelling results. EURAD-IM rather represents the event with two distinct dust clouds, following each other. Though, a detailed analysis of the analogy between Dust-RGBs from SEVIRI and the model results is not possible, since the satellite images are highly affected by thick clouds. These are associated with the cut-off low, which induced the dust emissions in the Sahara. Therefore, the clouds might obscure underlying mineral dust clouds.

4.3. AOD and surface concentration

Fig. 6 presents the comparison between the AOD observed by AERONET and the AOD modelled by both CTMs at 12 measurement sites distributed over the Iberian Peninsula, Mallorca, and Lampedusa (see their location in Fig. 3). The AOD is displayed for an observation wavelength of 550 nm as station-wise time series between 20 and 24 February. While the modelled AOD can be determined quasi-continuously by hourly model output regardless to persisting weather conditions, AERONET data only includes daytime AOD values, which

passed quality control and cloud screening. Therefore, the exact incidence of the dust event at the observation sites cannot always be identified. Short events (time-wise), like the one studied in this research paper, can be difficult to be observed and modelled for coincident time, and the limitation in measurements may not allow for checking time lags.

Both models are able to capture the general increase of AOD during the dust episode at all sites. On the other hand, both models do rarely capture the magnitude of the AOD as it is measured during the dust event. This is for example the case in Madrid, where the dust event with observations of up to 1.35 (21.02.2016) is strongly underestimated by the models (AOD_CHIMERE ≈ 0.20 and AOD_EURAD-IM ≈ 0.15). In Cabo da Roca, the AOD of observations and EURAD-IM coincide well. Here, CHIMERE partially underestimates the observed values with a root mean square error (RMSE) of 1.18. Additionally, CHIMERE shows a significant peak in the AOD around midnight on 21 February. However, there are no observations available for validation at this particular time. The evaluation of the model performance in Badajoz is also suffering

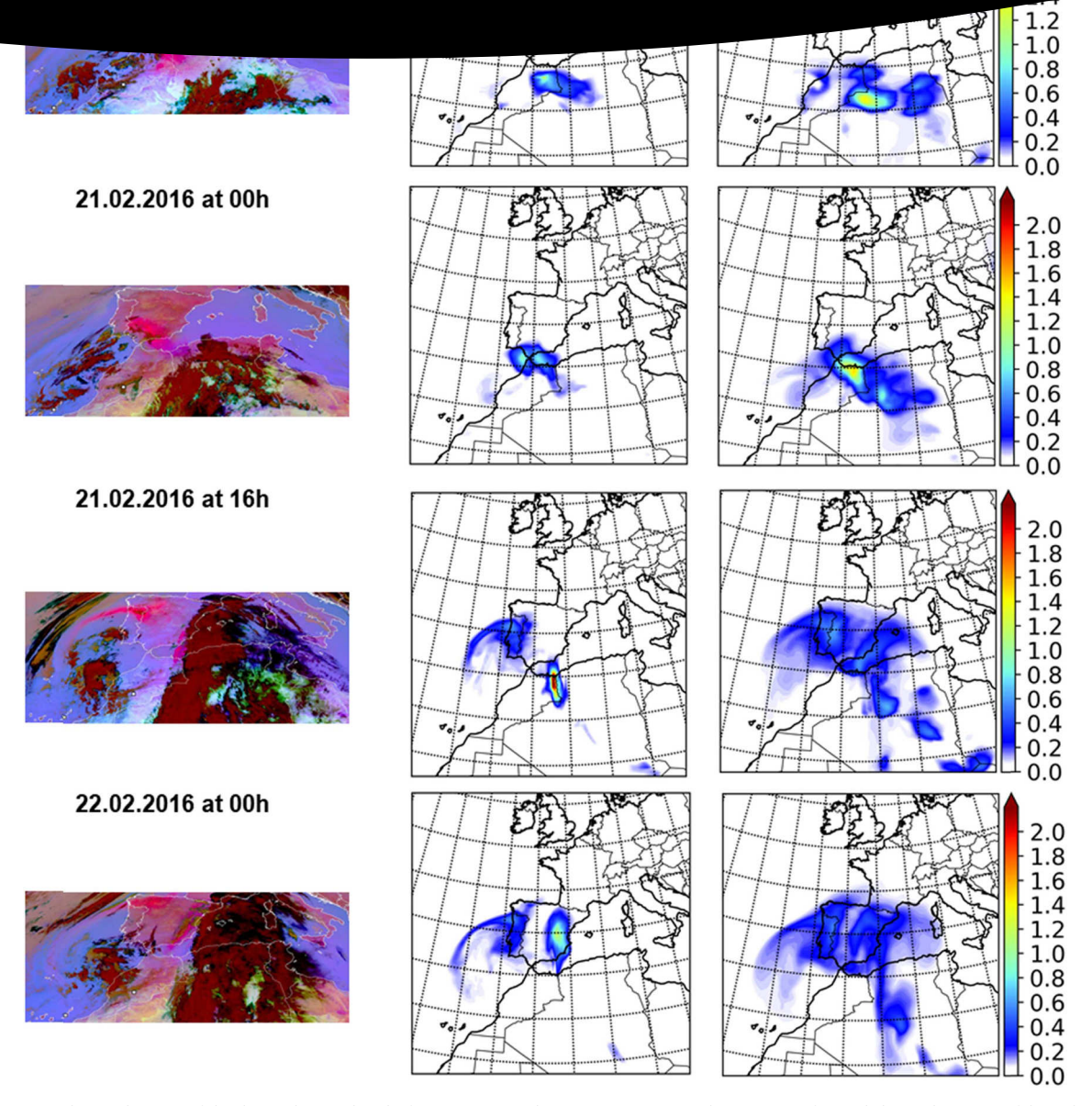


Fig. 5. Evolution and spatial extent of the desert dust outbreak (from 20 to 22 February 2016, at 16 and 00 UTC). Left panel shows the SEVIRI false colour Dust RGB product for part of the studied area and central and right panels show modelled AOD from EURAD-IM and CHIMERE, respectively. (For interpretation of the references to colour in this figure legend, the reader is referred to the Web version of this article.)

from missing AERONET observations, so that the AOD peaks of the models cannot be validated for early 21 February. The AOD peak of the observations in the morning of 21 February is not captured by the models, although if both show increased AOD values. Later on, during the decrease of AOD, the models match the observations fairly well.

Besides AOD, modelled PM10 and PM2.5 values are analysed to perform further validation exercises. The daily PM10 average concentrations simulated by both CTMs for the 21 and 22 February together with available monitored PM values observed at more than 20 locations are shown in Fig. 7. The results are presented by zooming the domain over Portugal, where the impact of the episode was strongest.

The transport and dispersion of mineral dust are simulated similarly

by both models, explained by the same meteorological forcing used (WRF simulation). However, the models simulate the magnitude of the dust episode differently. The production of dust is higher in CHIMERE in comparison to the dust emissions in EURAD-IM (see Section 4.1), that differences in terms of air quality can reach more than $100\,\mu g\,m^{-3}$ of PM10 in some regions (e.g. south of Portugal). Thus, CHIMERE results in maximum PM10 concentrations of about 230 $\mu g\,m^{-3}$ and EURAD-IM yields to at most $75\,\mu g\,m^{-3}$ on 22 February. These maximum concentrations appear in Southern Portugal, where good accordance of the observations and CHIMERE is given for daily PM10. In the wide area of Lisbon, where most observation sites are located, EURAD-IM rather represents the moderate burden of PM10. Regarding the daily PM2.5

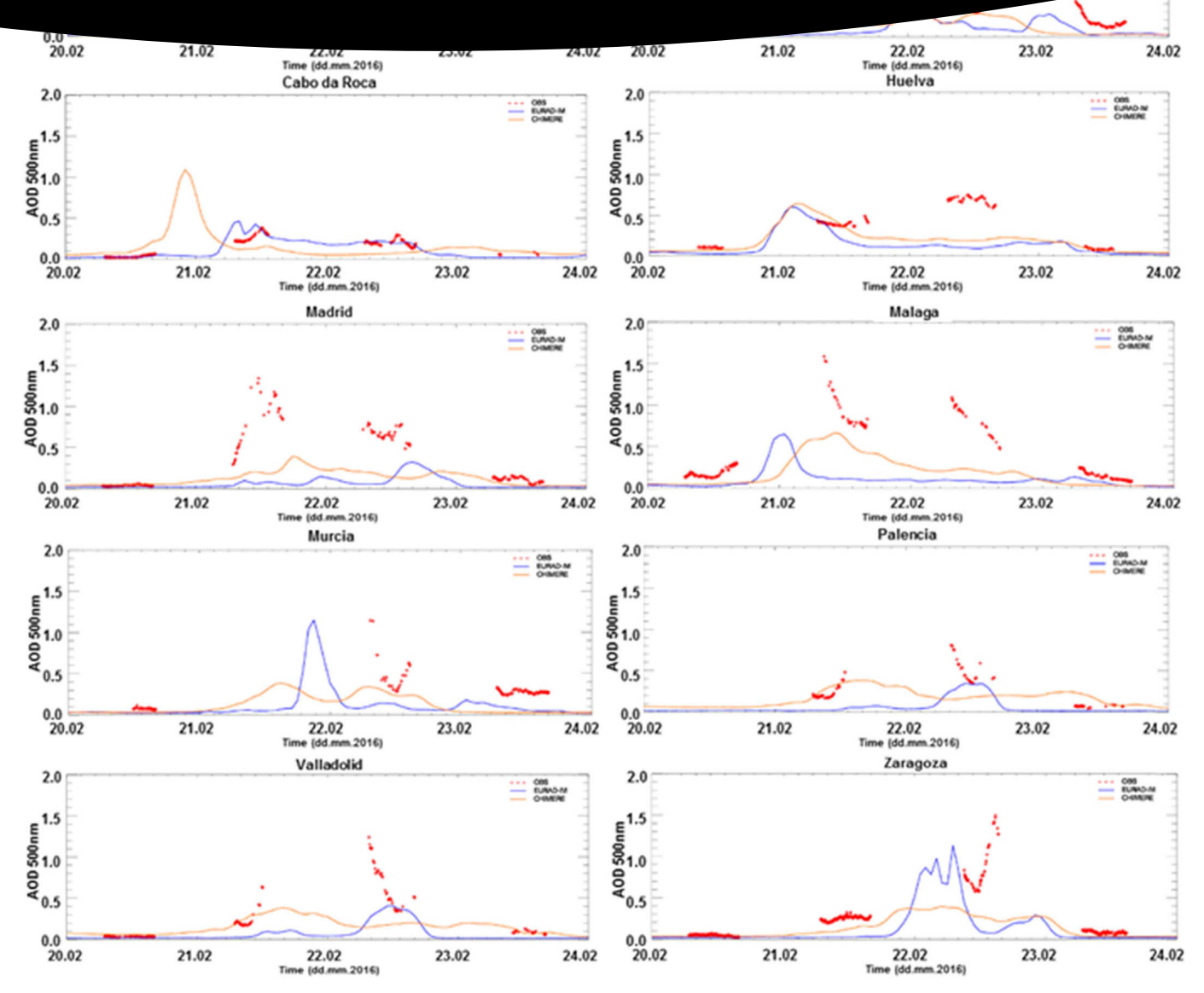


Fig. 6. AOD at 550 nm wavelength: observations from AERONET stations (red dots) versus AOD estimated by EURAD-IM (blue line) and CHIMERE (orange line). (For interpretation of the references to colour in this figure legend, the reader is referred to the Web version of this article.)

concentrations, both models perform well compared with the observations, with the exception that both models strongly underestimate the PM2.5 values of up to $100\,\mu g\,m^{-3}$ observed in south-east Portugal on 22 February.

Common model quality indicators, such as the Pearson correlation coefficient (Pearson's r), root mean square error (RMSE) and bias have been calculated (see Table 2), considering the hourly values modelled and observed in 22 background stations (rural, suburban or urban) in the case of PM10, and in 9 background stations in the case of PM2.5. Table 2 presents indicators relative to the period between February 15 to February 23, 2016, and assuming pairing in time but not in space. In addition, Fig. 8 shows the time series of hourly PM10 and PM2.5 concentrations modelled by the models and observations at selected monitoring stations (chosen to cover different regions and different

stations typology), during this unusually intense dust outbreak over Portugal.

Both models are able to correctly reproduce the magnitude of the PM10 values before the episode and the time of occurrence of the event with increased particulate matter burden in Portugal. In general, PM10 concentrations simulated by CHIMERE are higher than in EURAD-IM simulations. In the South of Portugal (TER and CER monitoring stations), CHIMERE shows better agreement with observations (RMSE_{CH-IMERE} = 33.9 $\mu g \ m^{-3}$; RMSE_{EURAD-IM} = 64.1 $\mu g \ m^{-3}$), while in the Centre Region (IGE, FUN and CHA monitoring stations), EURAD-IM performs better (for FUN, Pearson's $r_{\rm CHIMERE} = 0.60$; RMSE_{CHIMERE} = 61.1 $\mu g \ m^{-3}$; Pearson's $r_{\rm EURAD-IM} = 0.64$; RMSE_{EURAD-IM} = 22.0 $\mu g \ m^{-3}$).

Both models strongly underestimate PM2.5 concentrations during

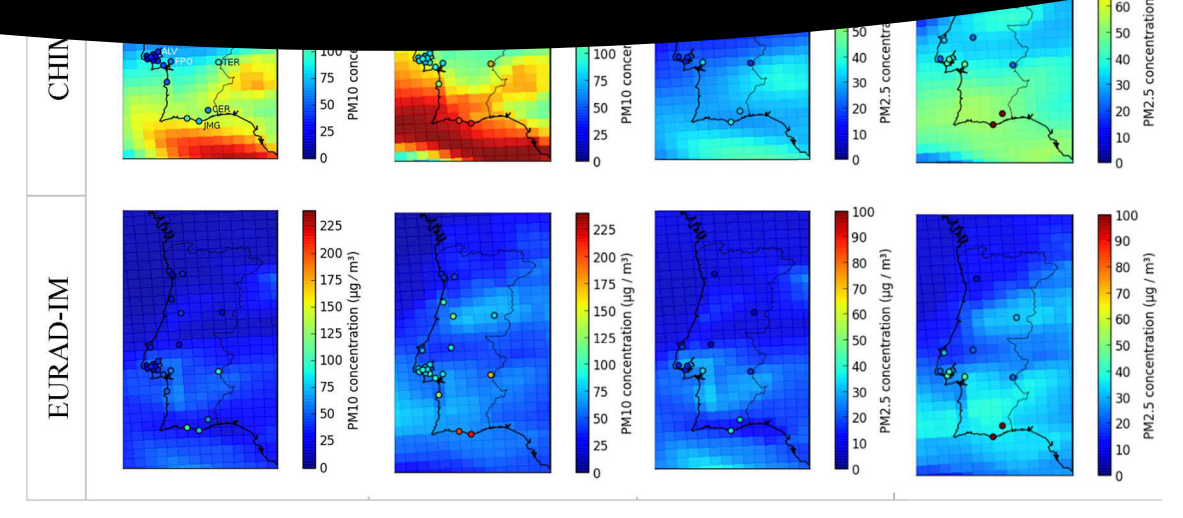


Fig. 7. Daily PM10 and PM2.5 averaged concentrations over Portugal on 21 and 22 February 2016: simulated by CHIMERE and EURAD-IM (gridded background) and observed at air quality monitoring stations (open circles).

Table 2Model quality indicators calculated with hourly concentrations observed/modelled from February 15 to February 23, 2016, in 22 background sites (9 for PM2.5), considering pairing in time but not in space.

Indicators	PM10	PM10		PM2.5	
	CHIMERE	EURAD-IM	CHIMERE	EURAD-IM	
Pearson's r RMSE (μg.m ⁻³) bias (μg.m ⁻³)	0.81 29.7 0.9	0.71 27.7 -13.3	0.79 10.3 -2.1	0.71 11.0 -3.5	

the dust event in southern Portugal (JMG and CER monitoring stations), as can be seen in Fig. 8. During the dust event, differences between hourly observations and models and reach maximum values close to $100\,\mu g\,m^{-3}$ (for the whole period of simulation, bias_CHIMERE = $-9.0\,\mu g\,m^{-3}$; bias_EURAD-IM = $-11.3\,\mu g\,m^{-3}$). The EURAD-IM performs especially well in the wide area of Lisbon (FPO monitoring station), simulating the two observed PM2.5 concentration peaks during the dust episode very well (see Fig. 8). However, both models are not able to simulate the daily fluctuations of PM2.5 before the dust arrival, probably related with local anthropogenic sources. Although the simulations include an estimation of anthropogenic emissions, the study resolution is too coarse to reproduce PM concentrations over urban areas.

4.4. Vertical profiles

Finally, modelling results are compared in terms of the vertical distribution of dust concentrations. Fig. 9 shows a sequence of profiles of simulated dust concentrations above Évora, Portugal (38.0°N, 7.9°W). The Saharan dust layer is located at higher atmospheric levels on 21 February at 03 UTC (between 750 and 500 hPa, according to CHIMERE simulation). The dust layer then descends towards surface levels, affecting particulate matter observations registered at the air quality monitoring stations after 21 February at 09 UTC (Fig. 8). During daytime (15 UTC) dust concentrations increase close to the surface,

which is probably related to the daily growth of the atmospheric boundary layer and consequent entrainment of dust-rich air from above. In particular, the TER monitoring station is located very close to Évora and shows a strong increase of particulate matter during the afternoon hours of the day.

Both models are able to predict the subsidence of the dust layer during this episode. The dust plume and its dust concentration is however again higher in CHIMERE than in EURAD-IM.

The strength of this event of February 2016 in terms of impact in air quality (PM10 and PM2.5 concentrations), with PM10 daily limit values for the protection of human health (50 μgm^{-3}) being surpassed throughout mainland Portugal, may be related to the strong subsidence at low levels of the atmosphere (Fig. 9). A similar event is reported by Cabello et al. (2012) that took place in October 2008 and had the strongest impact at ground level ever recorded in southern Spain.

5. Summary and conclusions

The EURAD-IM and CHIMERE CTMs have been applied to a strong desert dust event that occurred in February 2016 and affected air quality over Portugal severely. In the South of the country, observed PM10 concentrations reached hourly values above $200\,\mu g\,m^{-3}$, while PM2.5 reached values above $100\,\mu g\,m^{-3}$. Both modelling systems are able to capture the occurrence of the event (both models with a Pearson's r>0.7 for PM10 and PM2.5 concentrations), which was driven by a cut-off low off the coast of Morocco. This cyclone induced a strong meridional transport of dust loaden air from Algeria straight towards eastern parts of the Iberian Peninsula and further onwards to Portugal.

The most notable differences between the EURAD-IM and CHIMERE outputs concern the emission intensity (strength) and the emission source regions. EURAD-IM predicts smaller dust emission strengths than CHIMERE. According to EURAD-IM, dust is mainly emitted by loam soils, while CHIMERE predicts more emissions from sandy soils. Hence, EURAD-IM mainly computes dust emission source regions in Northern Algeria, while CHIMERE includes emissions in diverse local regions, distributed all over Algeria and the neighbouring countries.

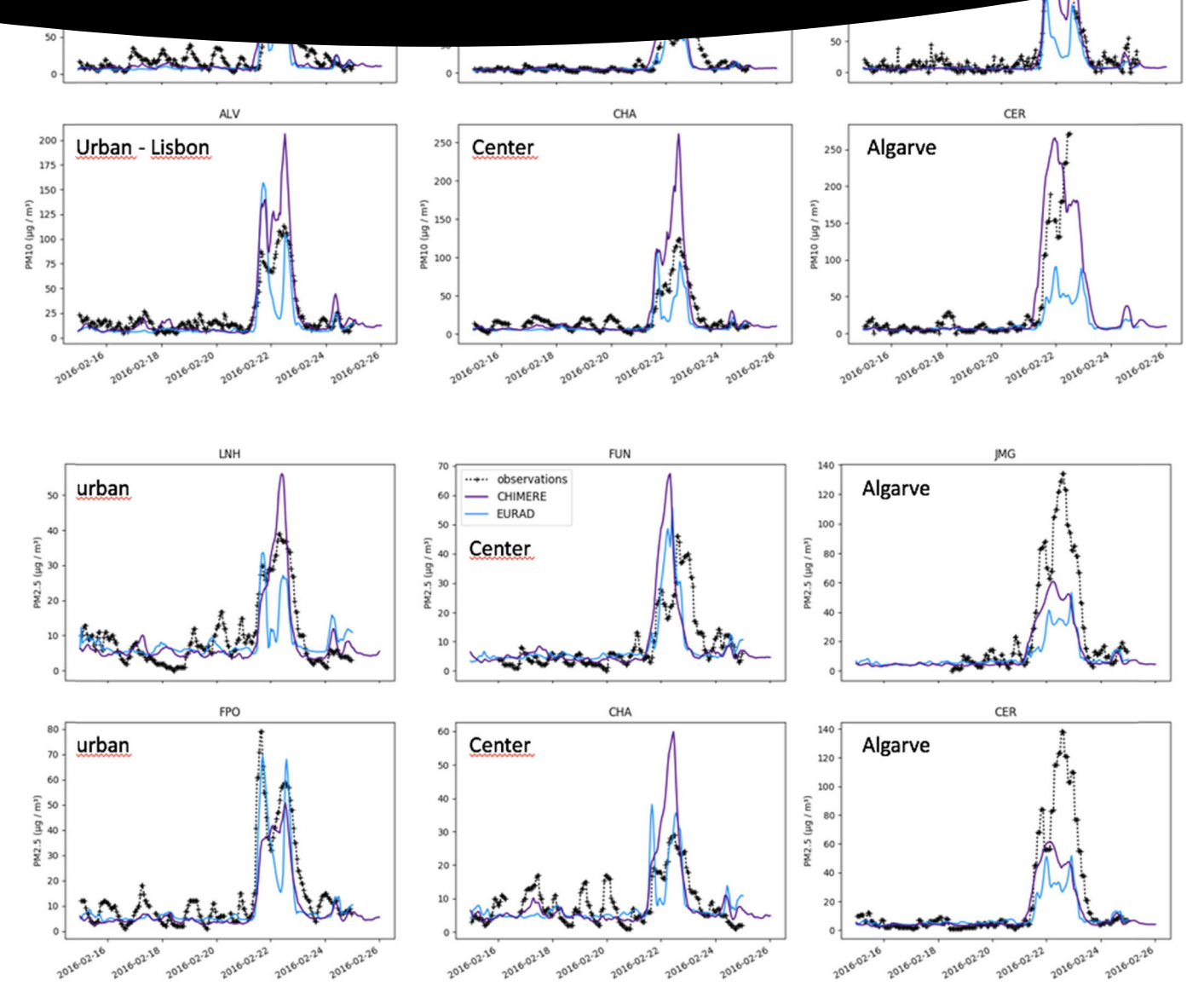


Fig. 8. Time series of hourly PM10 and PM2.5 concentrations from 15 to 26 February 2016: measured (black dashed line) and modelled by CHIMERE (purple line) and EURAD-IM (blue line) at six selected monitoring background stations in Portugal each (see their location in Fig. 7). (For interpretation of the references to colour in this figure legend, the reader is referred to the Web version of this article.)

These differences in emission strength and sources produces differences in terms of air quality and aerosol optical depths above the Iberian Peninsula. PM10 concentrations simulated by CHIMERE are higher than in EURAD-IM simulations (bias_{CHIMERE} = 0.9 $\mu g \, m^{-3}$; bias_{EURAD-IM} = $-13.3 \, \mu g \, m^{-3}$). In the South of Portugal, CHIMERE shows better agreement with ground observations (e.g., lower root mean square error), while in the centre region, EURAD-IM performs better. During the dust event, both models strongly underestimate PM2.5 concentrations in the South, where hourly observations and modelled concentrations reach maximum differences close to $100 \, \mu g \, m^{-3}$. Although the impact at the surface level is stronger in the South, model results and satellite data point out that higher dust contents in the total atmospheric column is located in the Centre of

Portugal

Both models, CHIMERE and EURAD-IM, show advantages in diverse times, locations, and quantities. The main difference between the simulation performances of the selected dust event is probably due to the differences of the algorithms for mineral dust uptake, which allow for strongly diverse source regions and consequently also emission strengths. Missing observations in the source region, originating from absent measurement sites and cloud coverage during the uptake of mineral dust by satellite observations, prevent a more detailed analysis of the emission characteristics. Nevertheless, the comparisons between the two models and the (limited) in-situ measurements allow to conclude that the different levels of PM concentrations found between the two models along the time of the episode are in part associated to the

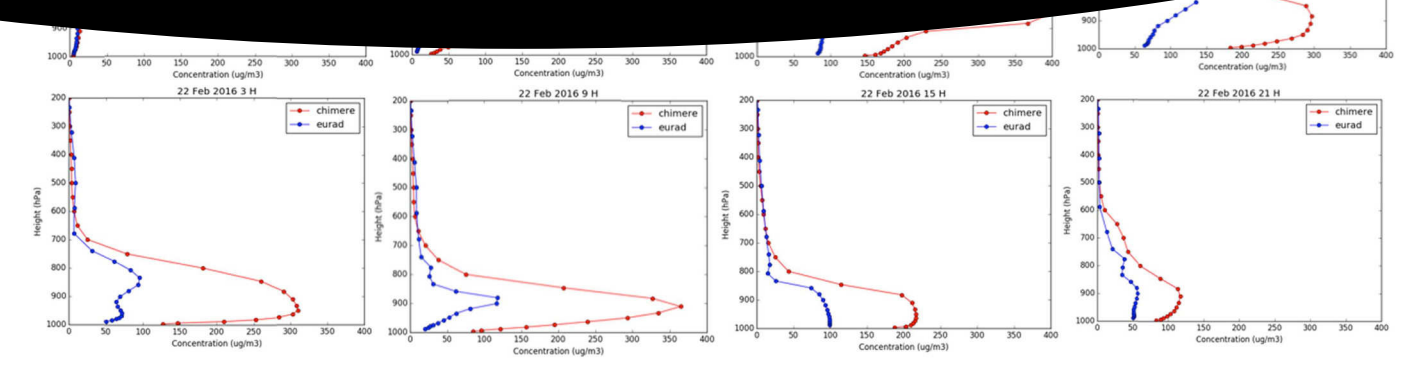


Fig. 9. Evolution of the vertical profiles of dust concentrations, produced with CHIMERE (red line) and EURAD-IM (blue line) at 38.0°N, 7.9°W. (For interpretation of the references to colour in this figure legend, the reader is referred to the Web version of this article.)

different dust sources estimated by each model.

Acknowledgements

The authors gratefully acknowledge the Luso-German Integrated Action A31/16 (CRUP/DAAD PPP funding program) and the computing time granted by the John von Neumann Institute for Computing (NIC) and provided on the supercomputer JURECA at Jülich Supercomputing Centre (JSC). Thanks are also due for the financial support to *the COST Action CA16202*, to CESAM (UID/AMB/50017/2019) and to the Portuguese FCT/MCTES through national funds (OE).

We would like to acknowledge the AERONET network, from which aerosol optical depths have been retrieved. We also acknowledge the MSG mission scientists and associated EUMETSAT personnel for the production of the Dust-RGB product used in this work.

References

Ackermann, I.J., Hass, H., Memmesheimer, M., Ebel, A., Binkowski, F.S., Shankar, U., 1998. Modal aerosol Dynamics model for Europe: development and first applications. Atmos. Environ. 32, 2981–2999. https://doi.org/10.1016/S1352-2310(9800006-5).

Agacayak, T., Kindap, T., Unal, A., Pozzoli, L., Mallet, M., Solmon, F., 2015. A case study for Saharan dust transport over Turkey via RegCM4.1 model. Atmos. Res. 153, 392–403. https://doi.org/10.1016/j.atmosres.2014.09.012.

Alfaro, S.C., Gomes, L., 2001. Modeling mineral aerosol production by wind erosion: emission intensities and aerosol size distributions in source areas. J. Geophys. Res. 106, 18075–18084. https://doi.org/10.1029/2000JD900339.

Balkanski, Y., Schulz, M., Claquin, T., Guibert, S., 2007. Reevaluation of Mineral aerosol radiative forcings suggests a better agreement with satellite and AERONET data. Atmos. Chem. Phys. 7, 81–95. https://doi.org/10.5194/acp-7-81-2007.

Bessagnet, B., Hodzic, A., Vautard, R., Beekmann, M., Cheinet, S., Honore, C., Liousse, C., Rouil, L., 2004. Aerosol modeling with CHIMERE - preliminary evaluation at the continental scale. Atmos. Environ. 38, 2803–2817. https://doi.org/10.1016/j. atmoseny.2004.02.034.

Bessagnet, B., Menut, L., Aymoz, G., Chepfer, H., Vautard, R., 2008. Modeling dust emissions and transport within Europe: the Ukraine March 2007 event. J. Geophys. Res.-Atmos. 113, D15. https://doi.org/10.1029/2007JD009541.

Bott, A., 1989. A Positive Definite Advection Scheme Obtained by Nonlinear Renormalization of the Advective Fluxes. Mon. Weather Rev. 117, 1006–1015. https://doi.org/10.1175/1520-0493(1989)117 < 1006:APDASO > 2.0.CO;2.

Cabello, M., Orza, J.A.G., Barrero, M.A., Gordo, E., Berasaluce, A., Cantón, L., Dueñas, C., Fernández, M.C., Pérez, M., 2012. Spatial and temporal variation of the impact of an extreme Saharan dust event. J. Geophys. Res. 117, D11204. https://doi.org/10.1029/2012JD017513.

Cazorla, A., Casquero-Vera, J.A., Román, R., Guerrero-Rascado, J.L., Toledano, C., Cachorro, V.E., Orza, J.A.G., Cancillo, M.L., Serrano, A., Titos, G., Pandolfi, M., Alastuey, A., Hanrieder, N., Alados-Arboledas, L., 2017. Near-real-time processing of a ceilometer network assisted with sun-photometer data: monitoring a dust outbreak over the Iberian Peninsula. Atmos. Chem. Phys. 17, 11861–11876. https://doi.org/10.5194/acp-17-11861-2017.

Chen, S.Y., Huang, J.P., Zhao, C., Qian, Y., Leung, L.R., Yang, B., 2013. Modeling the transport and radiative forcing of Taklimakan dust over the Tibetan Plateau: a case study in the summer of 2006. J. Geophys. Res.-Atmos. 118, 797–812. https://doi.org/ 10.1002/jord.50122

De Longueville, F., Hountondji, Y., Henry, S., 2010. What do we know about effects of desert dust on air quality and human health in West Africa compared to other regions? Sci. Total Environ. 409, 1–8. https://doi.org/10.1016/j.scitotenv.2010.09.

Elbern, H., Strunk, A., 2006. Chemical data assimilation for air quality forecasting. Proc. ECMWF Semin. Earth Obs. 285–296.

Elbern, H., Strunk, A., Schmidt, H., Talagrand, O., 2007. Emission rate and chemical state estimation by 4-dimensional variational inversion. Atmos. Chem. Phys. 7, 3749–3769. https://doi.org/10.5194/acp-7-3749-2007.

Elbern, H., Schwinger, J., Botchorishvili, R., 2010. Chemical state estimation for the middle atmosphere by four-dimensional variational data assimilation: system configuration. J. Geophys. Res. 115, D06302. https://doi.org/10.1029/2009JD011953.

Engelstaedter, S., Kohfeld, K.E., Tegen, I., Harrison, S.P., 2003. Controls of dust emissions by vegetation and topographic depressions: an evaluation using dust storm frequency data. Geophys. Res. Lett. 30, 1294. https://doi.org/10.1029/2002GL016471.

Escudero, M., Castillo, S., Querol, X., Avila, A., Alarcón, M., Viana, M.M., Alastuey, A., Cuevas, E., Rodríguez, S., 2005. Wet and dry African dust episodes over eastern Spain. J. Geophys. Res. 110, D18S08. https://doi.org/10.1029/2004JD004731.

European Commission, 2011. Commission Staff Working Paper Establishing Guidelines for Demonstration and Subtraction of Exceedances Attributable to Natural Sources under the Directive 2008/50/EC on Ambient Air Quality and Cleaner Air for Europe SEC(2011) 208 Final. Brussels 15.02.2011.

Forster, P., Ramaswamy, V., Artaxo, P., Berntsen, T., Betts, R., Fahey, D.W., Haywood, J., Lean, J., Lowe, D.C., Myhre, G., Nganga, J., Prinn, R., Raga, G., Schulz, M., Van Dorland, R., 2007. Radiative forcing of climate change. In: Solomon, S., Qin, D., Manning, M., Chen, Z., Marquis, M., Averyt, K.B., Tignor, M., Miller, H.L. (Eds.), Climate Change 2007: the Physical Science Basis. Contribution of Working Group I to the Fourth Assessment Report of the Intergovernmental Panel on Climate Change. Cambridge Univ. Press, Cambridge, United Kingdom and New York, NY, USA, pp. 129–234

Friese, E., Fröhlich, L., Elbern, H., Plu, M., Guidottu, S., Assar, N., 2017. Documentation of the EURAD-IM Regional System and Half-Yearly Report on the Development Activities (REF: CAMS50_2015SC2_D50.2.1.1.EURAD-IM-2017S1_201709_Dvpt_report_v1).

Gama, C., Tchepel, O., Baldasano, J.M., Basart, B., Ferreira, J., Pio, C., Cardoso, J., Borrego, C., 2015. Seasonal patterns of Saharan dust over Cape Verde – a combined approach using observations and modelling. Tellus B 67, 24410. https://doi.org/10. 3402/tellusb.v67.24410.

Ginoux, P., Chin, M., Tegen, I., Prospero, J.M., Holben, B., Dubovik, O., Lin, S.J., 2001. Sources and distributions of dust aerosols simulated with the GOCART model. J. Geophys. Res.-Atmos. 106, 20255–20273. https://doi.org/10.1029/2000JD000053.

Grell, G.A., Peckham, S.E., Schmitz, R., McKeen, S.A., Frost, G., Skamarock, W.C., Eder, B., 2005. Fully coupled "online" chemistry within the WRF model. Atmos. Environ. 39, 6957–6975. https://doi.org/10.1016/j.atmosenv.2005.04.027.

Guelle, W., Balkanski, Y., Schulz, M., Marticorena, B., Bergametti, G., Moulin, C., Arimoto, R., Perry, K.D., 2000. Modeling the atmospheric distribution of mineral aerosol: comparison with ground measurements and satellite observations for yearly and synoptic time scales over the North Atlantic. J. Geophys. Res. 105, 1997–2012. https://doi.org/10.1029/1999JD901084.

Haustein, K., Pérez, C., Baldasano, J.M., Jorba, O., Basart, S., Miller, R.L., Janjic, Z., Black, T., Nickovic, S., Todd, M.C., Washington, R., Müller, D., Tesche, M., Weinzierl, B.,

- Mahowald, N., Miller, R.L., Wortette, J.J., Stier, P., Takemura, T., Zender, C., 2011. Global dust model intercomparison in AeroCom phase I. Atmos. Chem. Phys. 11, 7781–7816. https://doi.org/10.5194/acp-11-7781-2011.
- Israelevich, P., Ganor, E., Alpert, P., Kishcha, P., Stupp, A., 2012. Predominant transport paths of Saharan dust over the Mediterranean Sea to Europe. J. Geophys. Res. 117, D02205. https://doi.org/10.1029/2011JD016482.
- Kok, J.F., Mahowald, N.M., Fratini, G., Gillies, J.A., Ishizuka, M., Leys, J.F., Mikami, M., Park, M.-S., Park, S.-U., Van Pelt, R.S., Zobeck, T.M., 2014. An improved dust emission model Part 1: model description and comparison against measurements. Atmos. Chem. Phys. 14, 13023–13041. https://doi.org/10.5194/acp-14-13023-2014.
- Kuenen, J.J.P., Visschedijk, A.J.H., Jozwicka, M., Denier van der Gon, H.A.C., 2014. TNO-MACC_II emission inventory: a multi-year (2003–2009) consistent high-resolution European emission inventory for air quality modelling. Atmos. Chem. Phys. 14, 10963–10976. https://doi.org/10.5194/acp-14-10963-2014.
- Kumar, R., Barth, M.C., Pfister, G.G., Naja, M., Brasseur, G.P., 2014. WRF-Chem simulations of a typical pre-monsoon dust storm in northern India: influences on aerosol optical properties and radiation budget. Atmos. Chem. Phys. 14, 2431–2446. https://doi.org/10.5194/acp-14-2431-2014.
- Kurosaki, Y., Mikami, M., 2005. Regional difference in the characteristic of dust event in East Asia: relationship among dust outbreak, surface wind, and land surface condition. J. Meteorol. Soc. Jpn. 83A. 1–18. https://doi.org/10.2151/jmsi.83A.1.
- Lensky, I.M., Rosenfeld, D., 2008. Clouds-aerosols-precipitation satellite analysis tool (CAPSAT). Atmos. Chem. Phys. 8, 6739–6753. https://doi.org/10.5194/acp-8-6739-2008.
- Liao, H., Seinfeld, J.H., Adams, P.J., Mickley, L.J., 2004. Global radiative forcing of coupled tropospheric ozone and aerosols in a unified general circulation model. J. Geophys. Res.-Atmos. 109, D16207. https://doi.org/10.1029/2003JD004456.
- Liu, X., Ma, P.-L., Wang, H., Tilmes, S., Singh, B., Easter, R.C., Ghan, S.J., Rasch, P.J., 2016. Description and evaluation of a new four-mode version of the modal aerosol module (MAM4) within version 5.3 of the community atmosphere model. Geosci. Model Dev. (GMD) 9, 505–522. https://doi.org/10.5194/gmd-9-505-2016.
- Mailler, S., Menut, L., Khvorostyanov, D., Valari, M., Couvidat, F., Siour, G., Turquety, S., Briant, R., Tuccella, P., Bessagnet, B., Colette, A., Létinois, L., Markakis, K., Meleux, F., 2017. CHIMERE-2017: from urban to hemispheric chemistry-transport modeling. Geosci. Model Dev. (GMD) 10, 2397–2423. https://doi.org/10.5194/gmd-10-2397-2017.
- Marticorena, B., Bergametti, G., 1995. Modeling the atmospheric dust cycle: 1. Design of a soil-derived dust emission scheme. J. Geophys. Res. 100, 415–430. https://doi.org/ 10.1029/95JD00690.
- Meloni, D., di Sarra, A., Monteleone, F., Pace, G., Piacentino, S., Sferlazzo, D.M., 2008. Seasonal transport patterns of intense Saharan dust events at the Mediterranean island of Lampedusa. Atmos. Res. 88, 134–148. https://doi.org/10.1016/j.atmosres. 2007.10.007.
- Menut, L., Bessagnet, B., Khvorostyanov, D., Beekmann, M., Blond, N., Colette, A., Coll, I., Curci, G., Foret, G., Hodzic, A., Mailler, S., Meleux, F., Monge, J.L., Pison, I., Siour, G., Turquety, S., Valari, M., Vautard, R., Vivanco, M.G., 2013. CHIMERE 2013: a model for regional atmospheric composition modelling. Geosci. Model Dev. (GMD) 6, 981–1028. https://doi.org/10.5194/gmd-6-981-2013.
- Menut, L., Foret, G., Bergametti, G., 2007. Sensitivity of mineral dust concentrations to the model size distribution accuracy. J. Geophys. Res. 112, D10210. https://doi.org/ 10.1092/2006.D007766
- Miller, R.L., Cakmur, R.V., Perlwitz, J., Geogdzhayev, I.V., Ginoux, P., Koch, D., Kohfeld, K.E., Prigent, C., Ruedy, R., Schmidt, G.A., Tegen, I., 2006. Mineral dust aerosols in the NASA goddard institute for Space Sciences ModelE atmospheric general circulation model. J. Geophys. Res.-Atmos. 111, D06208. https://doi.org/10.1029/2005JD005796.
- Mitsakou, C., Kallos, G., Papantoniou, N., Spyrou, C., Solomos, S., Astitha, M., Housiadas, C., 2008. Saharan dust levels in Greece and received inhalation doses. Atmos. Chem. Phys. 8, 7181–7192. https://doi.org/10.5194/acp-8-7181-2008.
- Monteiro, A., Fernandes, A.P., Gama, C., Borrego, C., Tchepel, O., 2015. Assessing the mineral dust from North Africa over Portugal region using BSC-DREAM8b model. Atmos. Pol. Res. 6, 70–81. https://doi.org/10.5094/APR.2015.009.
- Nickovic, S., Kallos, G., Papadopoulos, A., Kakaliagou, O., 2001. A model for prediction of desert dust cycle in the atmosphere. J. Geophys. Res.-Atmos. 106, 18113–18129. https://doi.org/10.1029/2000JD900794.
- Nieradzik, L.P., 2005. Application of a High Dimensional Model Representation on the Atmospheric Aerosol Module MADE of the EURAD-CTM. Master Thesis. Institut fur Geophysik und Meteorologie der Universitat zu Koln.

- over the Mediterranean Basin during 2001-2011: PM10 concentrations, phenomenology and trends, and its relation with synoptic and mesoscale meteorology. Atmos. Chem. Phys. 13, 1395–1410. https://doi.org/10.5194/acp-13-1395-2013.
- Reddy, M.S., Boucher, O., Balkanski, Y., Schulz, M., 2005. Aerosol optical depths and direct radiative perturbations by species and source type. Geophys. Res. Lett. 32, L12803. https://doi.org/10.1029/2004GL021743.
- Rizza, U., Barnaba, F., Miglietta, M., Gobbi, G., Mangia, C., Di Liberto, M., Dionisi, D., Costabile, F., Grasso, F., 2017. WRF-Chem model simulations of a dust outbreak over the central Mediterranean and comparison with multi-sensor desert dust observations. Atmos. Chem. Phys. 17, 93–115. https://doi.org/10.5194/acp-17-93-2017.
- Roselle, S., Binkowski, F., 1999. Capter 11: Cloud Dynamics and Chemistry, in Science Algorithms of the EPA Models–3 Community Multiscale Air Quality (CMAQ) Modeling System, EPA Report EPA/600/R–99/030.
- Rosenfeld, D., Rudich, Y., Lahav, R., 2001. Desert dust suppressing precipitation: a possible desertification feedback loop. Proc. Natl. Acad. Sci. U.S.A. 98, 5975–5980. https://doi.org/10.1073/pnas.101122798.
- Salvador, P., Artíñano, B., Molero, F., Viana, M., Pey, J., Alastuey, A., Querol, X., 2013. African dust contribution to ambient aerosol levels across central Spain: characterization of long-range transport episodes of desert dust. Atmos. Res. 127, 117–129. https://doi.org/10.1016/j.atmosres.2011.12.011.
- Salvador, P., Alonso-Pérez, S., Pey, J., Artíñano, B., de Bustos, J.J., Alastuey, A., Querol, X., 2014. African dust outbreaks over the western Mediterranean Basin: 11-year characterization of atmospheric circulation patterns and dust source areas. Atmos. Chem. Phys. 14, 6759–6775. https://doi.org/10.5194/acp-14-6759-2014.
- Sajani, Z., Miglio, R., Bonasoni, P., Cristofanelli, P., Marinoni, A., Sartini, C., Goldoni, C.A., De Girolamo, G., Lauriola, P., 2011. Saharan dust and daily mortality in Emilia-Romagna (Italy). Occup. Environ. Med. 68, 446–451. https://doi.org/10.1136/oem. 2010.058156.
- Schroedter-Homscheidt, M., Elbern, H., Holzer-Popp, T., 2010. Observation operator for the assimilation of aerosol type resolving satellite measurements into a chemical transport model. Atmos. Chem. Phys. 10, 10435–10452. https://doi.org/10.5194/ acp-10-10435-2010.
- Shao, Y., Wyrwoll, K.-H., Chappel, A., Huang, J., Lin, Z., McTainsh, G., Mikami, M., Tanaka, T., Wang, X., Yoon, S., 2011. Dust cycle: an emerging core theme in earth system science. Aeolian Res 2, 181–204. https://doi.org/10.1016/j.aeolia.2011.02. 001.
- Stafoggia, M., Zauli-Sajani, S., Pey, J., Samoli, E., Alessandrini, E., Basagaña, X., Cernigliaro, A., Chiusolo, M., Demaria, M., Díaz, J., Faustini, A., Katsouyanni, K., Kelessis, A.G., Linares, C., Marchesi, S., Medina, S., Pandolfi, P., Pérez, N., Querol, X., Randi, G., Ranzi, A., Tobias, A., Forastiere, F., MED-PARTICLES Study Group, 2016. Desert dust outbreaks in Southern Europe: contribution to daily PM10 concentrations and short-term associations with mortality and hospital admissions. Environ. Health Perspect. 124, 413–419. https://doi.org/10.1289/ehp.1409164.
- Tegen, I., Fung, I., 1994. Modeling of mineral dust in the atmosphere: sources, transport, and optical thickness. J. Geophys. Res. 99, 22897–22914. https://doi.org/10.1029/94JD01928
- Van Leer, B., 1979. Towards the ultimate conservative difference scheme. A second order sequel to Godunov's method. J. Computational Phys. 32, 101–136. https://doi.org/ 10.1016/0021-9991(79)90145-1.
- Vautard, R., Bessagnet, B., Chin, M., Menut, L., 2005. On the contribution of natural Aeolian sources to particulate matter concentrations in Europe: testing hypotheses with a modelling approach. Atmos. Environ. 39, 3291–3303.
- Washington, R., Todd, M., Middleton, N.J., Goudie, A.S., 2003. Dust-storm source areas determined by the total ozone monitoring spectrometer and surface observations. Ann. Assoc. Am. Geogr. 93, 297–313. https://doi.org/10.1111/1467-8306.9302003.
- Woodage, M.J., Slingo, A., Woodward, S., Comer, R.E., 2010. U.K. HiGEM: simulations of desert dust and biomass burning aerosols with a high-resolution atmospheric GCM. J. Clim. 23, 1636–1659. https://doi.org/10.1175/2009JCLI2994.1.
- Zhang, L., Gong, S., Padro, J., Barrie, L., 2001. A size-segregated particle dry deposition scheme for an atmospheric aerosol module. Atmos. Environ. 35, 549–560. https:// doi.org/10.1016/S1352-2310(00)00326-5.
- Zhang, L., Brook, J.R., Vet, R., 2003. A revised parameterization for gaseous dry deposition in air-quality models. Atmos. Chem. Phys. 3, 2067–2082. https://doi.org/10.5194/acm-3-2067-2003
- Zhao, C., Liu, X., Leung, L.R., Johnson, B., McFarlane, S.A., Gustafson Jr., W.I., Fast, J.D., Easter, R., 2010. The spatial distribution of mineral dust and its shortwave radiative forcing over North Africa: modeling sensitivities to dust emissions and aerosol size treatments. Atmos. Chem. Phys. 10, 8821–8838. https://doi.org/10.5194/acp-10-8821-2010.